Attention modulates spatial priority maps in human occipital, parietal, and frontal cortex

Thomas C. Sprague[1] and John T. Serences[1,2]

[1]Neuroscience Graduate Program, University of California San Diego
[2]Department of Psychology, University of California San Diego

Supplemental Material, including:

10 Figures

2 Tables

Supplementary Results

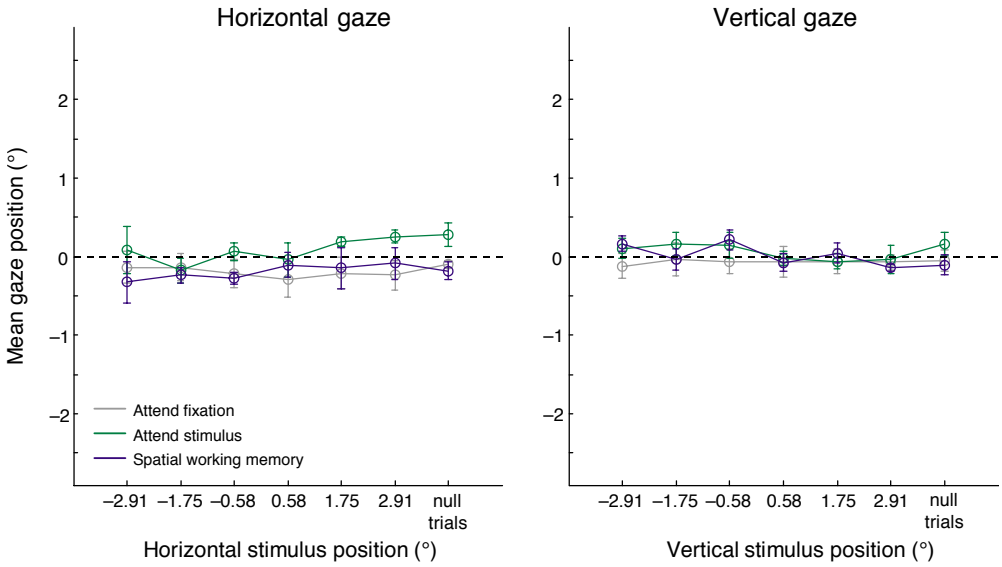

Supplementary Figure 1 Participants maintained fixation in the scanner during all three task conditions, related to Figure 2. Average horizontal and vertical gaze position across each 3 s trial in each task condition. Neither horizontal nor vertical gaze varied as a function of either stimulus position or task demands. 2-way ANOVA for each gaze direction, with task condition and stimulus position (grouped into 6 bins corresponding to *x* or *y* coordinate for horizontal and vertical gaze plots, respectively) as factors: minimum *p* for main effects/interactions = 0.2725, which was for main effect of vertical stimulus position on vertical gaze. Note that data from null trials were not entered into the ANOVA, but subjects maintained steady fixation on these trials as well. Eyetracking data gathered in the scanner for 4 of the 8 participants. Error bars ±1 S.E.M. across subjects.

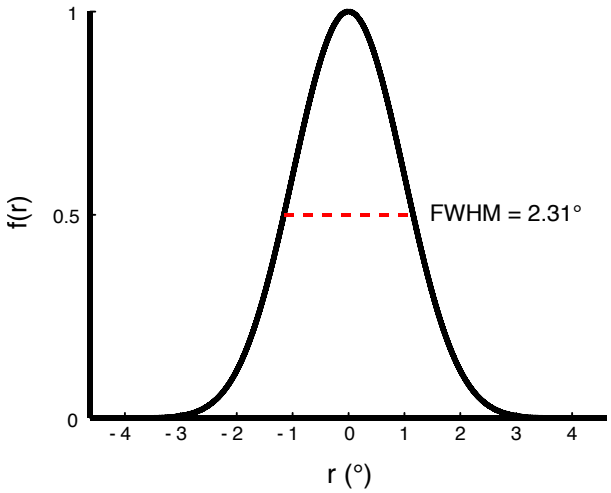

Supplementary Figure 2 One-dimensional cross-section of 2D basis function, related to Figure 3. Cross-section through the center of a single basis function (**Figure 3a**). FWHM is the full-width at half-maximum. The size constant, *s*, was set to $5r_{stim}$ (see Online Methods: *Encoding model*, **Supplementary Fig. 3**), where r_{stim} is 1.17°. This corresponds to the distance from the center at which the filter amplitude reaches 0.

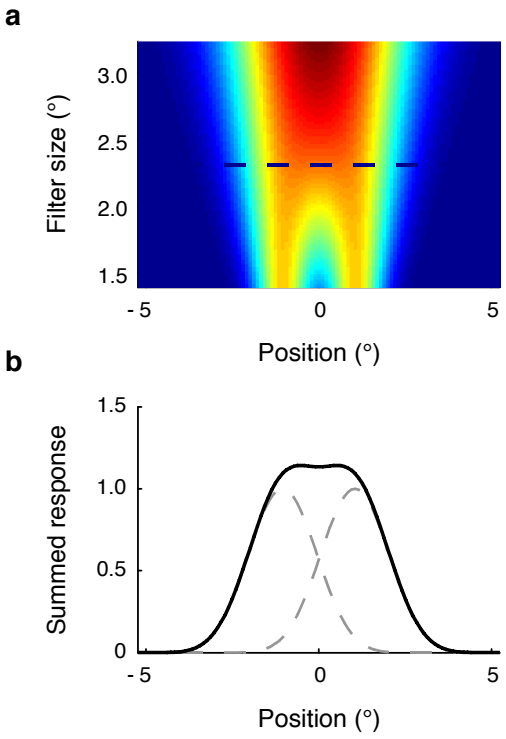

Supplementary Figure 3 The relationship between basis function size and spacing changes the smoothness of reconstructions, related to Figures 3 and 4. (**a**) For a constant spatial filter separation distance of 2.09° (which matches that used in the main analysis), we varied the size parameter (**Supplementary Fig. 2**) of 2 neighboring spatial filters, then plotted their sum as a function of position in space and filter size (which was continuously varied). Summed response is indicated by the image colorscale. (**b**) A slice from (**a**) at the FWHM of the filters used in the main analysis (dashed line in panel **a**). This value resulted in smooth reconstructions to which we could accurately fit surfaces to quantify the spatial representations (see Online Methods: *Curvefitting*), but also resulted in sufficient filter separation so that adjacent filters did not excessively overlap (see below). Smaller FWHM values would result in speckled reconstructed spatial representations which would be poorly fit using a single surface (this would be seen as a dipped black solid line in panel **b**; see panel **a** at small filter size values), and larger FWHM values would result in poorly discriminable predicted channel responses because neighboring filters would account for much of the same variance in the signal due to a high degree of overlap (see **a**, high FWHM values). At high enough FWHM values, the model cannot be estimated because overly high correlations between adjacent filters result in a rank deficient design matrix (Equation 1 in Online Methods).

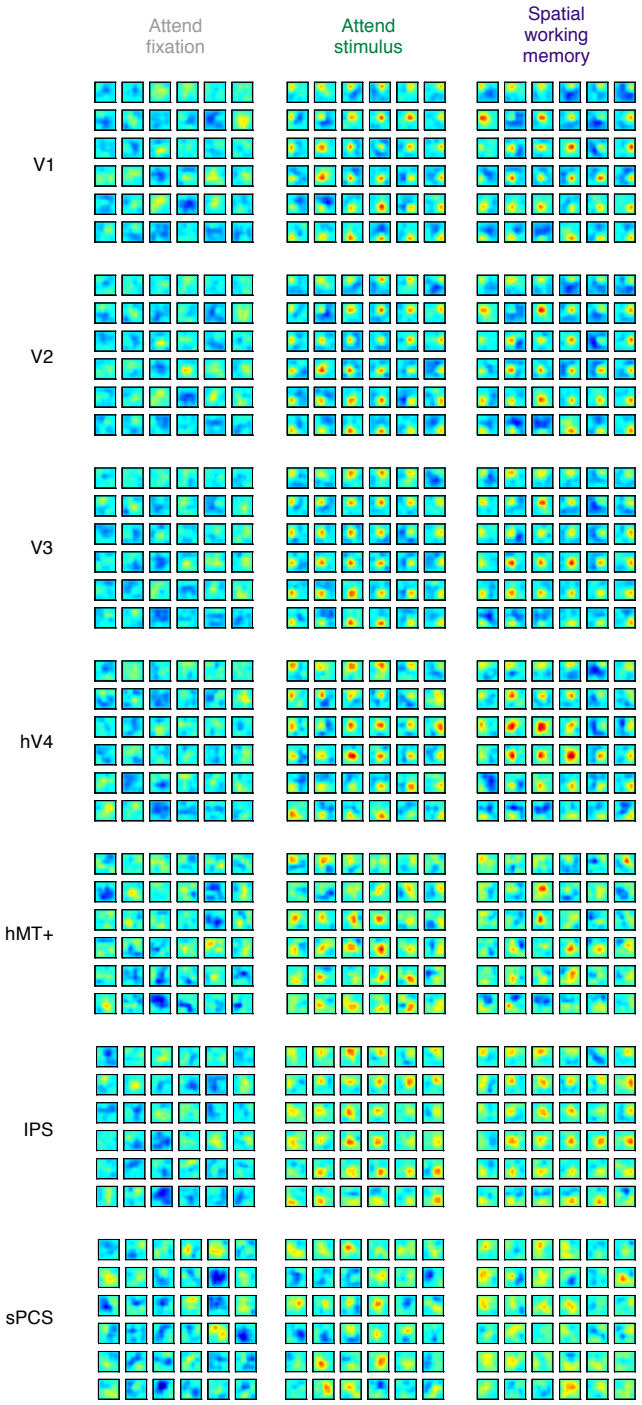

Supplementary Figure 4 Poor reconstructions during attend fixation condition for participant AG3, related to Figure 4. Plotted as in **Figure 4**. All images on same color scale. Poor reconstructed spatial representations were measured during attend fixation runs across all ROIs, but more typical looking reconstructed spatial representations were observed for both of the other task conditions. Behavioral performance for this participant indicated they were awake and vigilantly performing the fixation task. This was the only participant with this issue, and their data were not included in **Figures 4** or **5** (see Online Methods: *Excluded participant*). Note that the same estimated channel weight matrix was used here as was used to reconstruct spatial representations during the attend stimulus and spatial working memory tasks. Furthermore, note that these data support our conclusion of higher amplitude spatial priority maps with attention and they were excluded solely because of the noisy fits in the fixation condition. All of our reported effects would be more pronounced if this participant was included (see data included in the html version of this report).

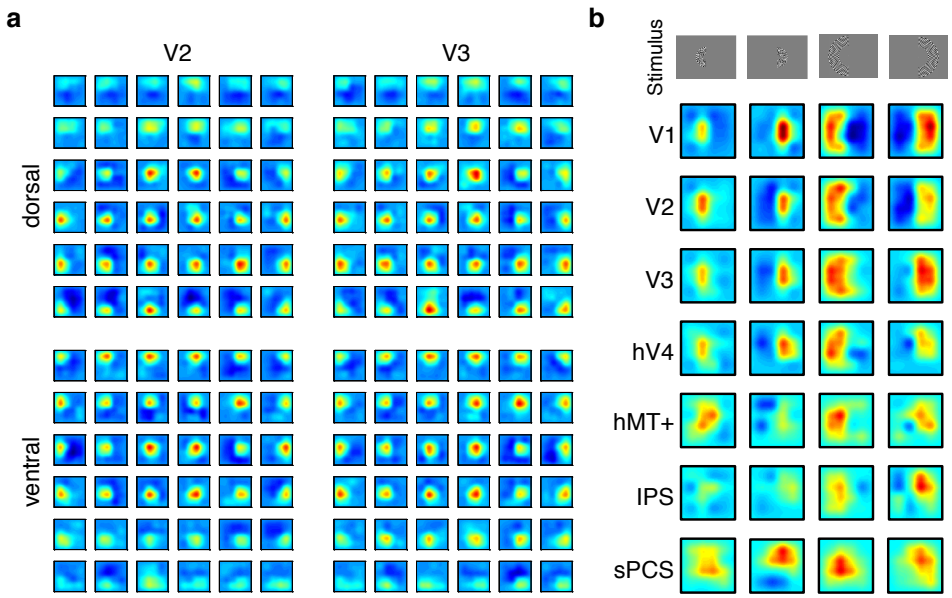

Supplementary Figure 5 Encoding model does not overfit data and generalizes to novel stimuli, related to Figure 4. (**a**) Reconstructions from all 36 stimulus locations under the attend stimulus condition across all 8 observers using voxels from only the ventral and dorsal aspects of V2 and V3. Color scale is identical to that used in Figure 4. Note that spatial reconstructions in the dorsal & ventral aspects of V2 and V3 are more robust in the lower and upper visual field, respectively. This pattern matches the known selectivity of dorsal and ventral areas V2 and V3. (**b**) Encoding model can be generalized to reconstruct novel stimuli that were not part of the *training set*. An encoding model trained using all attend fixation, attend stimulus & spatial working memory runs was able to accurately reconstruct a novel, untrained stimulus set acquired during a different scanning session on 7 of 8 participants presented in **Figures 4-5** (novel test data was not available for this 8th participant, AA3). This novel stimulus display consisted of four half-circle stimuli presented at one of two eccentricities (see top row), and the model was able to reconstruct these four stimuli with a high degree of precision (see Online Methods: *Stimulus reconstructions – novel stimuli* for more details).

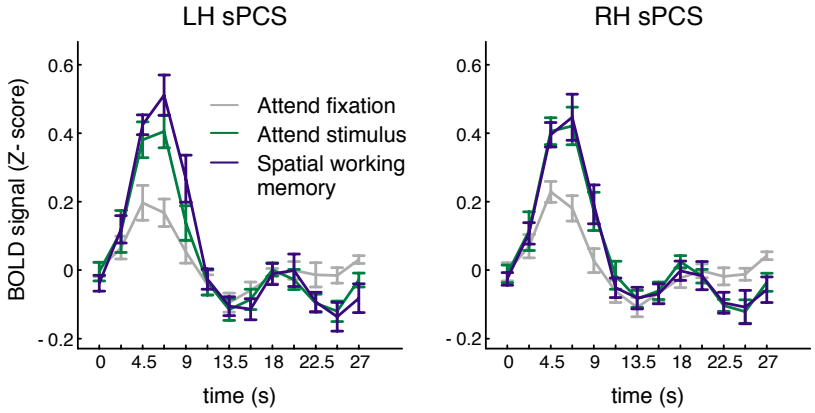

Supplementary Figure 6 sPCS exhibits larger responses, averaged across all voxels within the sPCS, in the attend stimulus and spatial working memory conditions, related to Figures 4 and 5. Both left and right sPCS exhibit strong hemodynamic responses to stimuli, with increased averaged (i.e. univariate) responses during attend stimulus and spatial working memory task conditions compared to the attend fixation condition. Additionally, this mean signal increase under conditions of attention to the stimulus or spatial working memory likely accounts for much of the significant increase in the baseline offset in the reconstructed stimulus representations reported in **Figure 5**. Error bars ±1 SEM across subjects.

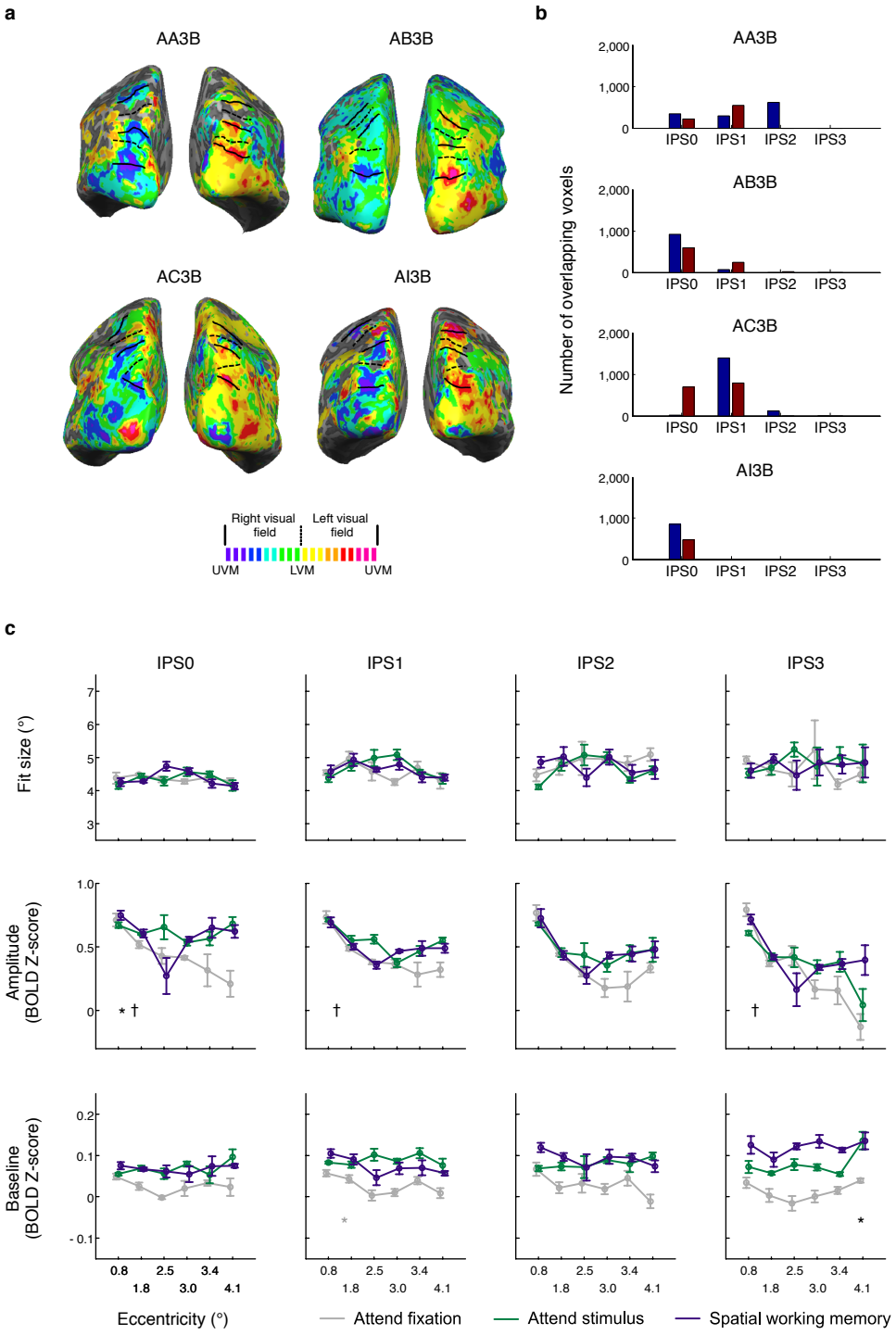

Supplementary Figure 7 IPS ROI primarily corresponds to IPS 0/1, related to Figures 6 and 7. (**a**) Polar angle preferences for each voxel plotted on the inflated surface of 4 participants' cortical sheets. Maps are liberally thresholded to show any voxel with normalized power at the stimulus frequency > 0.005. Smooth polar angle transitions were used to delineate four retinotopic regions of IPS (termed IPS 0-3) in each of these 8 hemispheres. Dashed lines: lower vertical meridian (LVM); solid lines: upper vertical meridian (UVM). (**b**) For each participant and each hemisphere we compared the number of overlapping voxels between our original localizer-defined IPS ROI (see Online Methods: *Mapping IPS subregions*) and each of these 4 retinotopically mapped IPS subregions . The original IPS ROI primarily overlaps with areas IPS 0 and 1, and is therefore

labeled as such in **Figure 7**. Blue: left hemisphere, Red: right hemisphere. (**c**) Fit parameters to reconstructed spatial representations estimated from activation patterns across each IPS subregion for these 4 participants (analysis identical to that implemented for **Fig. 7**). Critically, fit parameters in all regions are similar to those observed for the original IPS subregion (**Fig. 7**). Spatial representations of presented stimuli do not narrow in size when stimuli are attended or a target is remembered, but amplitude increases for representations in IPS0 ($p = 0.012$), and baseline increases in IPS3 ($p = 0.002$; statistics as in **Figs. 5** & **7**; error bars within-participant S.E.M.)

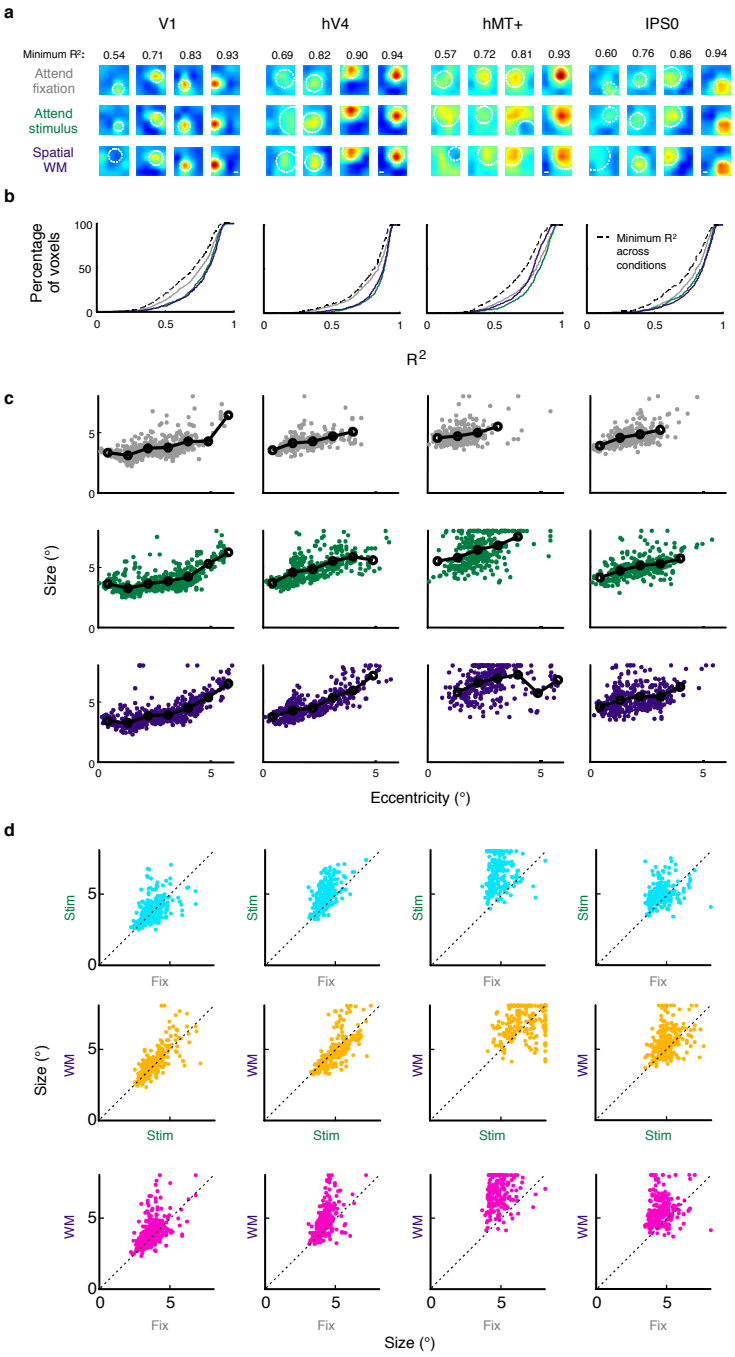

Supplementary Figure 8 Population receptive field analyses: example participant AA3B, related to Figure 7. (**a**) Reconstructed pRFs and best-fit isotropic function for voxels at each interquartile boundary. White dashed circles are plotted at half-maximum of fit function. Quartiles were split by minimum R^2 across all task conditions (see Online Methods: *Population receptive field estimation*). Above each column of pRFs is the minimum R^2 value across the 3 conditions shown below. The right 3 columns (top 50%) are voxels that were included in subsequent analyses. White horizontal scale bars correspond to 1° visual angle. (**b**) Distribution of R^2 (colored lines) and minimum R^2 across conditions (black lines) for each voxel, plotted as a cumulative distribution. (**c**) Size vs. eccentricity for each condition for each ROI. Each data point corresponds to a single voxel. Black circles/lines are the mean size at each eccentricity bin which contains ≥ 5 voxels (these are the points which are included in **Supplementary Fig. 9a**). All slopes for this example participant are significantly >

0 after Bonferroni correction across all 48 tests (4 participants × 4 ROIs × 3 conditions, corrected $\alpha = 0.001$), except hMT+, spatial working memory condition ($p = 0.006$, see Online Methods: *Statistical Procedures*). (**d**) Distribution of pRF size for each voxel across condition pairs. The percentage of voxels which lie above the unity line (that is, the percentage of voxels for which the size increases) within a ROI and condition pair is used to evaluate whether task demands significantly change pRF size (see **Supplementary Fig. 9b**, Supplementary Results, Online Methods).

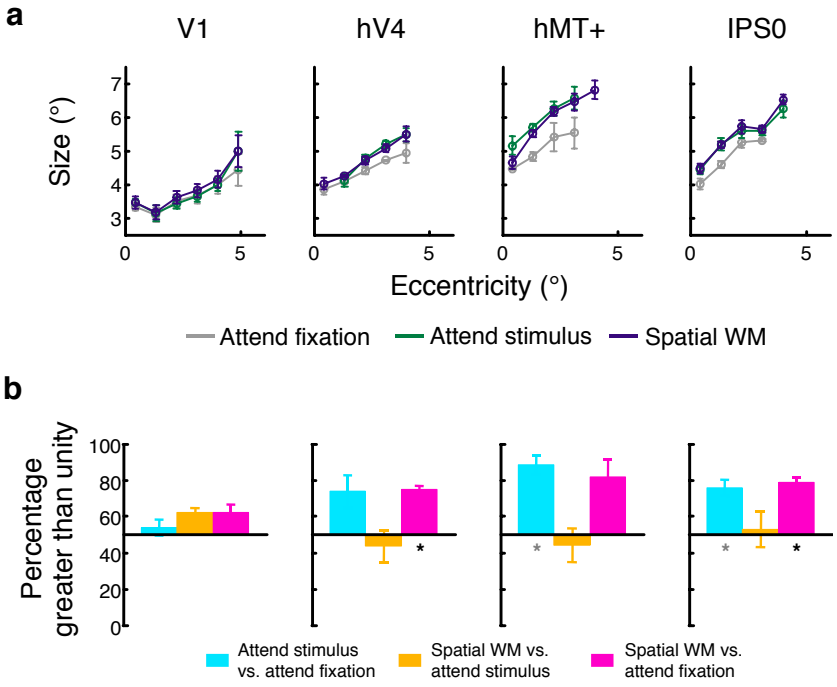

Supplementary Figure 9 Population receptive fields increase size with attention, related to Figure 7. (**a**) Summary of pRF size as a function of eccentricity across $n = 4$ participants. Each data point is plotted if ≥ 3 participants each had ≥ 5 voxels within that eccentricity bin. Error bars S.E.M. across included participants. (**b**) Summary of pRF size changes across each condition pair. For each ROI for each participant, we computed the percentage of voxels in which the pRF size was greater for the first condition than the second (e.g., cyan bars indicate the percentage of voxels in which pRF size was greater for the attend stimulus condition than for the attend fixation condition; this corresponds to the percentage of voxels which lie above unity when plotted as in **Supplementary Fig. 8d**). Black asterisks indicate significant size changes across a condition pair for an ROI, Bonferroni-corrected (two-tailed t-test, see Online Methods: *Statistical procedures*). Gray asterisks indicate a significant size change using a one-tailed t-test. Error bars indicate S.E.M. across participants ($n = 4$).

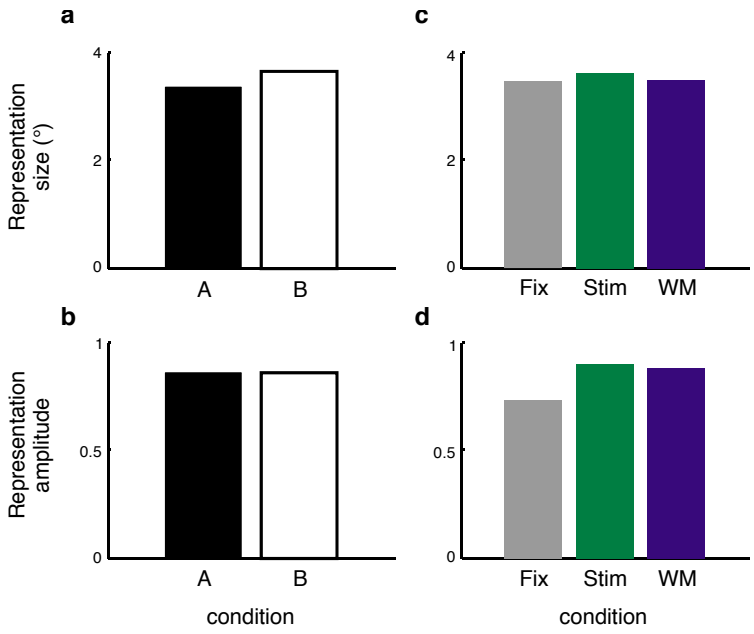

Supplementary Figure 10 Simulations demonstrate that uniform changes in voxel-level pRFs are reflected in changes in region-level spatial representations, related to Figure 7. (**a-b**) For 500 simulated voxels, we generated data for 2 conditions in which we only manipulated the simulated pRF size (condition B uses pRFs that were on average 11% larger than pRFs in condition A, which corresponds to the measured increase in pRF size between "attend stimulus" and "attend fixation" conditions in hV4 across all 4 participants). Under these conditions, the size of the multivariate spatial representations scaled with pRF size (**a**, smaller *spatial representation* sizes in condition A than in condition B). However, note that in this scenario, there is no change in fit amplitude (**b**). This demonstrates that (1) multivariate spatial representations are sensitive to changes in pRF size, given that the changes occur uniformly across a region, and (2) that our analysis technique can detect size changes mediated by uniform changes in pRF size in the absence of amplitude changes, were they occurring. This rules out an important possibility that representation size changes might be occurring in our dataset, but they could be too small to measure (see Results: *Size of spatial representations across eccentricity and ROI*). (**c-d**) In panels **a-b** we demonstrate that multivariate region-level spatial representations can increase in size, reflecting uniform changes in the underlying univariate voxel-level pRFs. Here, we used the fit pRF parameters for 1 example participant (AA3B, shown in **Supplementary Fig. 8**) and 1 ROI (hV4), which undergo non-uniform size changes across conditions, to simulate data for all 3 task conditions in the main experiment. Even with pRF size increases observed across conditions (**Supplementary Fig. 8d**), multivariate spatial representations are shown to maintain a constant size (**c**), but increase in amplitude (**d**, mirroring our data in **Figs. 5, 7**). This pattern of results was also found in the other three participants (not shown). This demonstrates a decoupling of pRF size/amplitude and the size/amplitude of multivariate region-level spatial representations, and underscores the importance of exploiting all of the information available in a region to estimate the fidelity of spatial encoding.

	X	Y	Z	volume (mL)
RH-IPS	27.78 ± 3.37	-71.21 ± 4.23	29.33 ± 3.38	0.961 ± 0.37
LH-IPS	-26.80 ± 2.38	-71.32 ± 5.44	27.35 ± 4.30	1.301 ± 0.57
RH-sPCS	30.77 ± 6.36	-5.54 ± 5.00	49.67 ± 3.74	1.411 ± 0.37
LH-sPCS	-28.76 ± 4.22	-8.14 ± 4.44	46.95 ± 1.72	1.17 ± 0.28
RH-hMT+	39.54 ± 3.08	-66.15 ± 5.95	3.03 ± 4.06	1.01 ± 0.12
LH-hMT+	-43.79 ± 6.55	-70.31 ± 5.60	3.32 ± 4.97	0.894 ± 0.20

Supplementary Table 1 Mean ROI sizes and locations, related to Figures 4-5. Mean ± 1 standard deviation locations of ROI centers in Talairach coordinates and volumes for hMT+, IPS and sPCS ROIs.

Mean slope ± standard error across participants (significant participants/4)	**V1**	**hV4**	**hMT+**	**IPS0**
Attend fixation	0.332 ± 0.028 (4)	0.330 ± 0.038 (3)	0.484 ± 0.171 (3)	0.554 ± 0.032 (4)
Attend stimulus	0.381 ± 0.030 (4)	0.536 ± 0.039 (4)	0.621 ± 0.190 (3)	0.479 ± 0.031 (4)
Spatial WM	0.414 ± 0.055 (4)	0.495 ± 0.082 (4)	0.647 ± 0.148 (3)	0.451 ± 0.057 (4)

Supplementary Table 2 pRF size vs. eccentricity slope, related to Figure 7. Each cell contains mean slope in units of pRF size (°)/eccentricity (°), as well as the number of participants with significantly nonzero size vs. eccentricity slopes. All participants, regardless of significance, are included in the mean and standard error. Number of significant participants is evaluated using a Bonferroni-corrected alpha value for 48 comparisons of $\alpha = 0.001$.

Supplementary Results

Population receptive fields (pRFs)

As a complementary analysis, we identified pRFs for each voxel for each condition for a subset of participants and ROIs (see Online Methods: *Population receptive field estimation*). We restricted our analysis to the half of all voxels in each region for which reconstructed pRFs were well-fit with a unifocal isotropic function (**Supplementary Fig. 8a**). In our implementation of the pRF analysis, we reconstruct a map of the portion(s) of the visual field which best drive the BOLD response in each voxel (see **Supplementary Fig. 8a** for example pRFs in each ROI for 1 participant). Then, we fit a smooth 2d surface to each of these reconstructed pRFs, and use the best fit position and size to characterize pRF properties across different attention conditions (best fits shown by white circles in **Supplementary Fig. 8a**). Note that, while most fits appeared accurate, some "best" fits do not accurately capture the positive region of the pRF. To choose "good" fits without bias, we computed an R^2 value for each condition. Then for every voxel we used the minimum R^2 across conditions to determine a median R^2 for every ROI for every participant (**Supplementary Fig. 8b**). Voxels with minimum R^2 greater than or equal to the corresponding median value were included in subsequent analyses.

Because our stimulus set and analysis method was not designed to evaluate pRFs at the resolution that dedicated pRF mapping protocols are (e.g., ref 42), we found generally larger pRFs than have been observed previously. However, we replicated the key pRF result that pRF size increases with eccentricity (**Supplementary Fig. 8c**, **Supplementary Fig. 9a**). At least 3 of the 4 participants had significantly positive slopes for each condition/ROI pairing (see **Supplementary Table 2** for mean slopes and number of significant participants), and all significantly non-zero slopes were positive.

Next, we compared whether the best-fit pRF size increased or decreased in more voxels between each pair of task conditions (attend stimulus vs. attend fixation, spatial WM vs. attend stimulus and spatial WM vs. attend fixation). **Supplementary Fig. 8d** shows this analysis for an example participant. At the group level, the percentage of voxels which lie above the unity line (**Supplementary Fig. 9b**) changed as a function of condition pair (significant main effect of condition pair, $p = 0.007$), and we also observed a condition × ROI interaction ($p = 0.047$). In 2 of 3 regions in which we observed significant increases in the amplitude of spatial representations with attention (**Fig. 5**, hV4 and IPS), we also observed significant size increases in at least one condition pair (hV4: spatial WM vs. attend fixation, $p < 0.001$; IPS0: spatial WM vs. attend fixation, $p = 0.003$; all others n.s. after Bonferroni correction for 12 comparisons, $\alpha = 0.0042$).

Simulated spatial representations

When pRF size is uniformly modulated across conditions (**Supplementary Fig. 10a-b**), we observed changes in the size of spatial representations. Spatial representation size reflects changes in pRF size. When pRF size was increased by 11%, spatial representation size increased by 9.28%. Our analysis method is thus sensitive to particular types of pRF modulation with attention, and so if pRF size is uniformly decreasing or increasing, the measured size of multivariate spatial representations would shrink or expand as a result.

When we used best-fit pRFs to data from each condition from a single participant's hV4 ROI, in which pRF size non-uniformly increases, we observed stable spatial representation size across conditions, as well as an increase in amplitude of spatial representations across attention conditions (**Supplementary Fig. 10c-d**), mirroring our results from the main text (**Figs. 5**, **7**). This demonstrates that, while our analysis method is sensitive to changes in representation size as a result of uniform pRF modulation with attention (**Supplementary Fig. 10a**), such a modulation is not observed when we account for the more nuanced pattern of pRF modulations that is present in our dataset (**Supplementary Fig. 10c**). Additionally, these results demonstrate that while voxel-level univariate pRFs might be subject to particular types of modulation with attention, the size of multivariate region-level spatial representations can remain stable and either increase or decrease in amplitude. This result also underscores the importance of constraining estimates of modulations in spatial information content of a region by the modulatory pattern across all component units (voxel-level pRFs) within the region, as there is not a one-

to-one mapping of changes in pRF size/amplitude to changes in the size/amplitude of region-wide spatial representations.